Environment International 157 (2021) 106802

Contents lists available at ScienceDirect

Environment International

journal homepage: www.elsevier.com/locate/envint

Integrated multi-omics analysis reveals the underlying molecular mechanism for developmental neurotoxicity of perfluorooctanesulfonic acid in zebrafish

Hyojin Lee [a], Eun Ji Sung [b], Seungwoo Seo [c], Eun Ki Min [a], Ji-Young Lee [d], Ilseob Shim [d], Pilje Kim [d], Tae-Young Kim [c,1,2], Sangkyu Lee [b,1,2], Ki-Tae Kim [a,*]

[a] Department of Environmental Engineering, Seoul National University of Science and Technology, Seoul 01811, Republic of Korea
[b] BK21 FOUR Community-Based Intelligent Novel Drug Discovery Education Unit, College of Pharmacy and Research Institute of Pharmaceutical Sciences, Kyungpook National University, Daegu 41566, Republic of Korea
[c] School of Earth Sciences and Environmental Engineering, Gwangju Institute of Science and Technology, Gwangju 61005, Republic of Korea
[d] Environmental Health Research Department, National Institute of Environmental Research, Incheon 22689, Republic of Korea

ARTICLE INFO

Keywords:
Perfluorooctanesulfonic acid
Neurotoxicity
Multi-omics
Integration
Zebrafish

ABSTRACT

Limited studies on multi-omics have been conducted to comprehensively investigate the molecular mechanism underlying the developmental neurotoxicity of perfluorooctanesulfonic acid (PFOS). In this study, the locomotor behavior of zebrafish larvae was assessed under the exposure to 0.1–20 μM PFOS based on its reported neurobehavioral effect. After the number of zebrafish larvae was optimized for proteomics and metabolomics studies, three kinds of omics (i.e., transcriptomics, proteomics, and metabolomics) were carried out with zebrafish larvae exposed to 0.1, 1, 5, and 10 μM PFOS. More importantly, a data-driven integration of multi-omics was performed to elucidate the toxicity mechanism involved in developmental neurotoxicity. In a concentration-dependent manner, exposure to PFOS provoked hyperactivity and hypoactivity under light and dark conditions, respectively. Individual omics revealed that PFOS exposure caused perturbations in the pathways of neurological function, oxidative stress, and energy metabolism. Integrated omics implied that there were decisive pathways for axonal deformation, neuroinflammatory stimulation, and dysregulation of calcium ion signaling, which are more clearly specified for neurotoxicity. Overall, our findings broaden the molecular understanding of the developmental neurotoxicity of PFOS, for which multi-omics and integrated omics analyses are efficient for discovering the significant molecular pathways related to developmental neurotoxicity in zebrafish.

1. Introduction

Perfluorooctanesulfonic acid (PFOS) is representative of a legacy long-chain perfluoroalkyl and polyfluoroalkyl substances (PFAS), and for two decades of toxicological studies, PFOS has been a potent PFAS along with perfluorooctanoic acid. PFOS has been widely used as a versatile protector in fabric, leather, paper, semi-conductors, and fire-fighting foams for > 60 years (Kwon et al., 2014; Moody et al., 2002). Recently, as newly developed PFAS alternatives became available (Lin et al., 2017), the application of PFOS has been replaced and the toxicity of alternatives has gained attention. However, bio-monitoring studies indicated that, among legacy and emerging PFAS, PFOS had the highest concentration and greatest detection frequency in the environment and in fish samples (Valsechhi et al., 2021; Lee et al., 2020), and exposure concentrations in human serum were slowly reduced, in spite of restrictions established in the early 2000s (Olsen et al., 2017). Concerns about environmental impacts and human health problems caused by PFOS are still of critical importance.

The accumulating toxicological studies have revealed that PFOS causes multiple adverse effects, such as developmental toxicity,

* Corresponding author.
E-mail addresses: kimtaeyoung@gist.ac.kr (T.-Y. Kim), sangkyu@knu.ac.kr (S. Lee), ktkim@seoultech.ac.kr (K.-T. Kim).
[1] These authors contributed equally to this work.
[2] Co-correspondences authors at: College of Pharmacy and Research Institute of Pharmaceutical Sciences, Kyungpook National University, Daegu 41566, Republic of Korea (S. Lee). School of Earth Sciences and Environmental Engineering, Gwangju Institute of Science and Technology, Gwangju 61005, Republic of Korea (T.-Y. Kim).

https://doi.org/10.1016/j.envint.2021.106802
Received 31 May 2021; Received in revised form 19 July 2021; Accepted 26 July 2021
Available online 4 August 2021

hepatotoxicity, immunotoxicity, reproductive toxicity, endocrine disruption, cardiovascular toxicity, pulmonary toxicity, and renal toxicity (Tsuda, 2016; Zeng et al., 2019). Of particular interest is the potential of PFOS to cause neurotoxicity (Chen et al., 2014; Johansson et al., 2008a, 2008b), because PFOS can cross the blood–brain barrier (BBB) and accumulate in the brain (Andersen et al., 2006; Cui et al., 2009). In addition, exposure to PFOS during early life stages, including prenatal exposure, was reported to cause developmental neurotoxicity in models of murine and zebrafish. Recently, developmental neurotoxicity observed in zebrafish larvae was suggested to be the significant endpoint for judging PFAS toxicity, and PFOS was the most toxic to behavioral alteration (Gaballah et al., 2020). The various mechanisms that are reportedly involved in the neurotoxicity of PFOS were nerve cell damage; stimulation of neuroinflammation; alteration of the neurochemical transmission system; and disturbance of synaptogenesis, synaptic plasticity, and the calcium ion (Ca^{2+}) channel (Zeng et al., 2019; Yuan et al., 2018). However, limited studies on the molecular mechanism for the developmental neurotoxicity of PFOS have been conducted.

In zebrafish toxicology, omics techniques, which include transcriptomics, proteomics, and metabolomics, have been applied to explore holistic molecular perturbations by various toxic chemicals. However, single-omics-based technology is limited in providing a one-side change in the biomolecule (i.e., mRNA, protein, and metabolite), which impedes comprehensive understanding of toxicity mechanism and identification of molecular initiating events and key events for adverse outcome pathway development. To overcome these challenges, multi-omics approaches that employ at least two or more omics data have been suggested. Integration of multi-omics enables us to efficiently capture multifaceted networks from gene to phenotype and understand a train of toxic mechanisms. Attempts to consider multi-omics or integrated omics have increased (Buesen et al., 2017; Canzler et al., 2020; Wu et al., 2018; Lee et al., 2021). In the zebrafish model, transcriptomics (Martínez et al., 2019) and metabolomics (Ortiz-Villanueva et al., 2018) were applied to investigate developmental toxicity and endocrine disruption upon exposure to PFOS. The integrative multi-omics analysis would be helpful for unraveling the comprehensive molecular mechanism that underlies developmental neurotoxicity caused by PFOS treatment.

In the present study, we analyzed three kinds of omics (i.e., transcriptomics, proteomics, and metabolomics) and integrated datasets that were obtained from multi-omics by using a data-driven integration approach to further explore the neurotoxicity mechanism of PFOS in zebrafish. In particular, one experimental condition (i.e., the number of larvae) was optimized for instrumental proteomics and metabolomics analyses. With respect to the developmental neurotoxicity of PFOS, the individual omics- and integrated omics-based pathways were compared.

2. Materials and methods

2.1. Zebrafish husbandry and exposures

Adult wild-type zebrafish (AB, *Danio rerio*) aged to 10–13 months were maintained under standard husbandry conditions in a 14:10-h light:dark cycle at 28.5 °C in a flow-through culture system (Tecniplast, Buguggiate, Italy). Healthy embryos were obtained from spawning adult zebrafish. Embryos at a certain developmental stage were collected and placed in a Petri dish filled with E2 media and cultured in an incubator (28 °C) until toxicity evaluation. All animal procedures were approved by the Institutional Animal Care and Use Committees at the Seoul National University of Science and Technology.

All chemicals were purchased from Sigma-Aldrich (St. Louis, MO, USA). To investigate the underlying molecular mechanisms, PFOS exposure was designed with concentrations showing the neurotoxic impacts in previous studies (Ulhaq et al., 2013; Menger et al., 2020; Zhang et al., 2021). The PFOS exposure concentrations were 0, 0.1, 1, 5, 10, and 20 μM, including 0.1% dimethyl sulfoxide (DMSO). At 4 h post-fertilization (hpf), zebrafish embryos were individually transferred to 96-well plates and exposed to 100 μL PFOS solution until 120 hpf under light-blocking conditions. A total of 64 randomly selected larvae (16 larvae per replicate) was used in each concentration, and developmental toxicity was evaluated by recording the mortality and malformation under a microscope at 120 hpf. Exposure to PFOS for the locomotor response assay and omics analysis were carried out following the same aforementioned experimental conditions, such as 96-well plates, exposure period of 4–120 hpf, 0.1% DMSO, and 100 μL volume. The overall experimental workflow is described in detail in **Fig. S1**.

2.2. Locomotor response assay

A light/dark transition locomotor response assay has been utilized to assess the developmental neurotoxicity of chemicals in zebrafish (d'Amora and Giordani, 2018; Jin et al., 2021; Tran et al., 2021). A total of 32 larvae per concentration was used, and the dead or malformed larvae at 120 hpf were excluded from analysis. After acclimation in the dark phase for 10 min, the light/dark cycle (10-min light and 10-min dark phases) was repeated twice. The locomotor activity was analyzed using ZebraBox® (Viewpoint, Lyon, France), and the total distance moved was calculated under each photocycle. The detailed movement was evaluated for three swimming speeds: freezing $\leq$ 5 mm/s, cruising = 5–20 mm/s, and bursting $\geq$ 20 mm/s. Considering the results of developmental toxicity and locomotor response, 0, 0.1, 1, 5, and 10 μM PFOS concentrations were used for omics analysis. However, because few proteins and metabolites that were changed at 0.1 μM PFOS were discerned through proteomics and metabolomics, three concentrations of 1, 5, and 10 μM were evaluated for bioinformatic analysis.

2.3. Transcriptomics analysis

2.3.1. RNA extraction and pre-processing sequencing

After exposure to PFOS, 60 randomly selected zebrafish larvae (20 larvae per replicate) from each concentration were collected in 1.5-mL microtubes and homogenized with zinc beads using MagNa Lyzer (Roche Diagnostics, Basel, Switzerland). The total RNA (>200 ng) was extracted from homogenates using RNAzol® reagent (Molecular Research Center Inc., Cincinnati, OH, USA). RNA sequencing libraries were built using a TruSeq Stranded mRNA Sample Prep Kit (Illumina, San Diego, CA, USA). The sequencing library was quantified with a KAPA Library Quantification Kit and were analyzed as a paired end (2 × 100 bp) using the Illumina NovaSeq system. The library quality was evaluated using Agilent 2100 BioAnalyzer (Agilent, Santa Clara, CA, USA). Sequencing reads were filtered with a quality cutoff of 20 and a minimum length of 50. The filtered reads were aligned to the Ensembl reference genome on *Danio_rerio* (GCA_000002035.4). These mapping reads were utilized to calculate the expression level of transcripts with R tools such as RSEM v1.3.1, featureCounts v2.0.0, HTSeq-count v0.11.2, and Cufflinks v2.2.1.

2.3.2. Differentially expressed gene analysis

Differentially expressed genes (DEGs), which are genes with statistically significant differences between the control and PFOS-treated groups, were analyzed using Rstudio v1.3 equipped with the packages edgeR v3.28.1 and EnhancedVolcano. DEGs were determined on the basis of the criteria of significance (p-value < 0.05) and the expression level (absolute log2 fold change > 1.5). The enriched pathways on DEGs were analyzed with KEGG Database, Cytoscape v3.7.2, and ClueGO v2.5.7.

2.3.3. Validation using quantitative real-time polymerase chain reaction (qRT-PCR)

qRT-PCR analysis was performed to verify the RNA-seq data. Specific primers of genes related to neurotransmission were designed using NCBI Primer-BLAST (**Table S1**). cDNA was synthesized with the RNA extracts

that were used in the RNA-seq, using a High Capacity cDNA Reverse Transcription Kit (Thermo Fisher Scientific, Foster City, CA, USA). Analytical methods for qRT-PCR were described in our previous study (Lee et al., 2019).

2.4. Proteomics analysis

2.4.1. Protein sample preparation

The appropriate number of larvae in proteomics was evaluated using the extracts, which were obtained from 20, 50, and 100 larvae each, with duplication. Twenty larvae were the minimum at which the number of identified proteins were steady, and thus determined as the number of larvae for proteomics study. Protein extraction and identification were performed equally according to the following experimental protocols. Sixty embryos (20 larvae per replicate) determined through optimization were deyolked as previously described (Kimmel et al., 1995) and were exposed to 0.1, 1, 5, and 10 μM PFOS. Deyolked embryos were washed with phosphate-buffered saline and RIPA buffer supplemented with protease inhibitors, and phosphatase inhibitors were added. These mixed samples were homogenized through sonication and centrifuged at 16,000 × *g* for 10 min at 4 °C to remove the tissue debris, and the supernatants were collected. The protein concentration was quantified using a BCA protein assay (Thermo Fisher Scientific, Foster City, CA, USA), and protein extraction was ascertained through sodium dodecyl sulfate–polyacrylamide gel electrophoresis analysis. The extracted proteins were digested and modified to peptides. Digested peptides of 90 μg were labeled with 4-plex TMT labeling according to the manufacturer's protocol (Thermo Fisher Scientific, Foster City, CA,

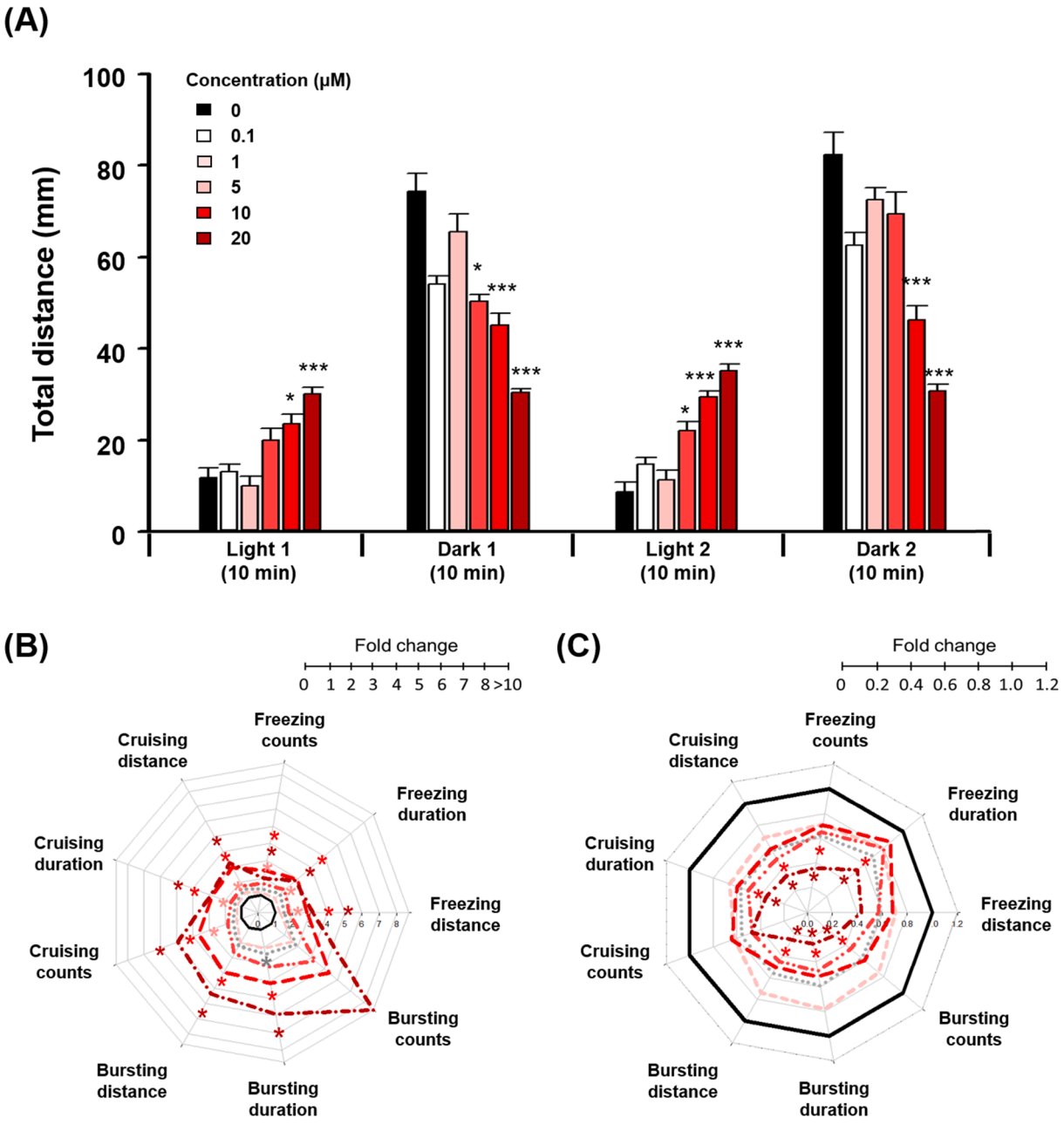

Fig. 1. Alteration of locomotor behavior of zebrafish exposed to PFOS. (A) The total distance moved are depicted by a light/dark transition. The radar graphs represent the fold change of movement in the distance, count, and duration of PFOS-treated groups compared to control in (B) the light phase and (C) dark phase. PFOS concentrations are described with 0 μM (black), 0.1 μM (white), 1 μM (light pink), 5 μM (dark pink), 10 μM (red), and 20 μM (dark red). Significance is denoted by $*p < 0.05$, $**p < 0.01$, and $***p < 0.001$. (For interpretation of the references to color in this figure legend, the reader is referred to the web version of this article.)

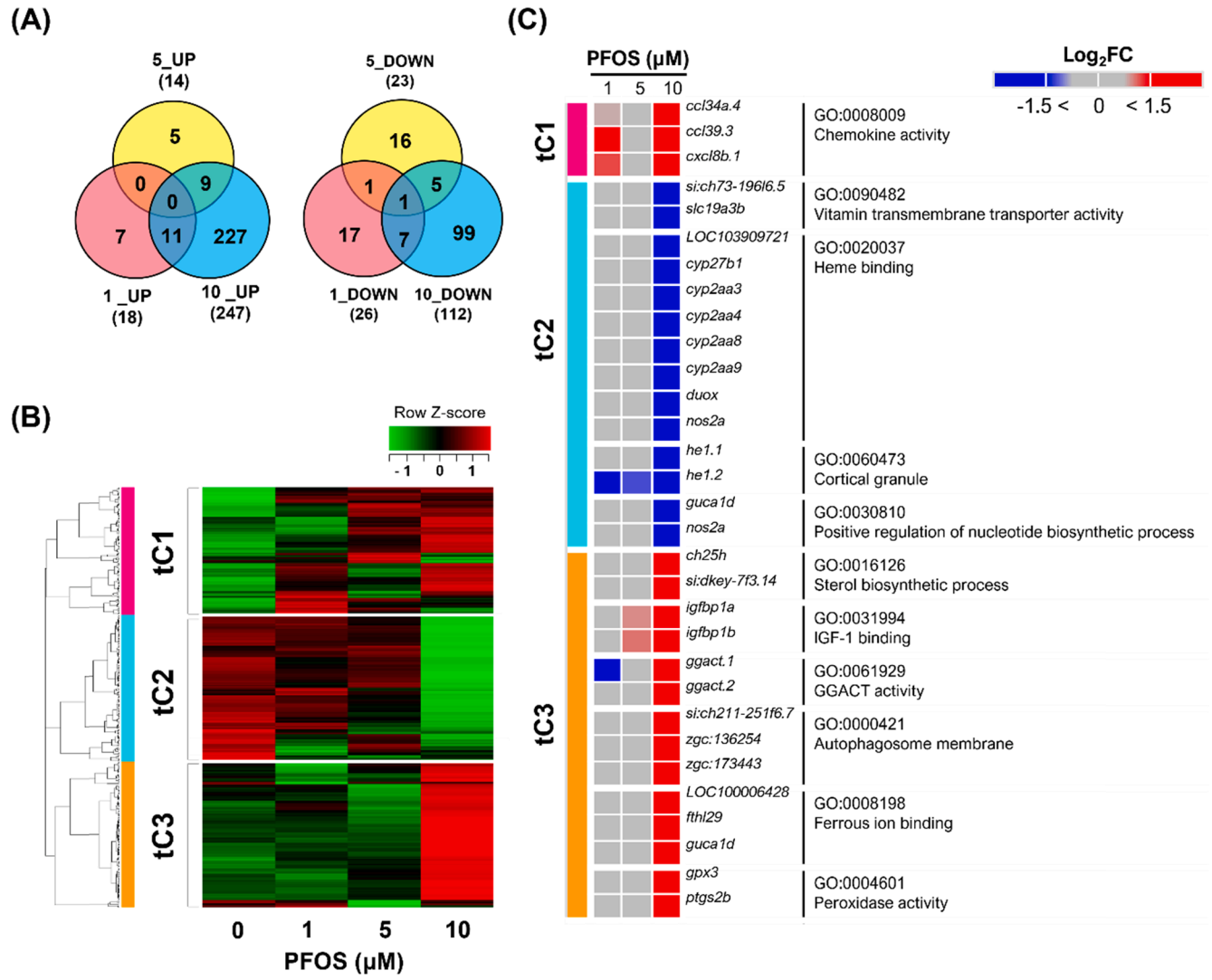

Fig. 2. Transcriptomic alteration. (A) Venn diagram and (B) heat map of differentially expressed genes are depicted. The number of DEGs shows in parenthesis of up- and down-regulation at each PFOS concentration. (C) Significant gene ontology pathways in transcriptomic Clusters 1–3 are described.

USA). The processes of protein digestion and peptide fractionation are described in detail in Method S1. The mass spectrometry proteomics data have been deposited to the ProteomeXchange Consortium via the PRIDE (Perez-Riverol et al., 2019) partner repository with the dataset identifier PXD025972.

2.4.2. Quantitative proteomic and bioinformatic analyses

Peptides from each fraction were dissolved in solvent A (water in 0.1% formic acid) and analyzed on an UltiMate 3000 RSLCnano LC system coupled with an LTQ-Orbitrap mass spectrometer (Thermo Fisher Scientific, Foster City, CA, USA). A peptide from each fraction was loaded via an Acclaim PepMap 100 trap C18 column (75 μm × 2 cm, 3 μm, and 100 Å) and ionization was achieved using an Easy Spray HPLC C18 column (50 cm). These columns were purchased from Thermo Fisher Scientific Inc. (Foster City, CA, USA). The obtained MS/MS spectra data were annotated and calculated as the ratio of report ions using the TMT 4-plex method at MaxQaunt 1.5. All other parameters in MaxQuant were set to default values. Differentially expressed proteins (DEPs) are defined as proteins with the fold change ratio < 0.8 (down-regulation) and > 1.8 (upregulation) on the basis of relative abundance compared to the control group. The enrichment pathways were analyzed using the list of the quantified proteins using DAVID v6.8 with a modified Fisher's exact test using a p-value < 0.05 and a minimum count of two. Detailed analysis conditions (e.g., LC conditions, MS scan, and peak annotation) are described in Method S1.

2.5. Metabolomic analysis

2.5.1. Metabolite extraction

The number of metabolites was optimized from untreated larvae of 20, 35, 50, and 100 each, with three replicates. The proper number of larvae (i.e., 50) was determined to be the minimum at which the number of metabolites was stable. Metabolite extraction and identification for optimization were carried out following the experimental protocols. A total of 150 zebrafish larvae exposed to PFOS (50 larvae per replicate) was randomly collected and prepared for each concentration. For metabolite extraction, 1 mL acetonitrile:isopropanol:water (3:3:2, v/v/v) was added to the sample vial. The mixture of solvent and sample was pulverized using a microtube pestle in a 1.5-mL Eppendorf tube. After centrifugation at 20,200 × g for 5 min at 4 °C, the supernatant was taken and dried using SpeedVac. The dried samples were stored at − 80 °C until further analysis.

2.5.2. Quantitative metabolomics analysis

Before LC-MS/MS analysis, all dried samples were re-dissolved in 100 μL of 50% aqueous acetonitrile and centrifuged at 20,200 × g for 10

min at 4 °C. The supernatant was used for LC-MS/MS analysis, which was performed using an Agilent Infinity 1260 LC system (Agilent, Santa Clara, CA, USA) coupled to an Agilent 6520 Q-TOF mass spectrometer with an electrospray ionization source. A Waters ACQUITY UPLC BEH column (2.1 × 100 mm and 1.7 μm) was used for chromatographic separation. The multi-group analysis function of XCMS online software was used to perform peak detection, peak alignment, and peak grouping for raw MS files with HPLC/Q-TOF preset parameters (Gowda et al., 2014), and metabolites were identified with a NIST17 library through MS/MS spectra. Differentially expressed metabolites (DEMs) were selected from the list by conducting a Kruskal–Wallis analysis in R (p-value < 0.05). Statistical analysis and pathway annotation, including partial least squares discriminant analysis (PLS-DA) and hierarchical clustering heatmap analysis, were performed on the DEM list using Metaboanalyst 5.0. Detailed information on the LC instrument conditions and metabolite identification are described in Method S2.

2.6. Multi-omics integration

Three datasets on significant molecules (i.e., DEGs, DEPs, and DEMs) were used for multi-omics analysis. Pairwise integration and association analysis (X ↔ Y, X ↔ Z, and Y ↔ Z) of three omics data were performed using a sparse partial least squares (SPLS) regression method in xMWAS v0.55 (Uppal et al., 2018). SPLS analysis performs simultaneous data integration and optimal variable selection, making it suitable for data with multitudinous features and a small sample size. xMWAS executes network visualization to provide topological distribution of nodes and a multilevel community detection algorithm to identify highly connected nodes, which represent significant molecules. After community detection, the pathways of each community were analyzed using database tools on transcripts (ClueGO v2.5.7), proteins (DAVID functional annotation tool v6.8), and metabolites (Metaboanalyst v5.0). The top six pathways in each cluster were determined on the basis of the $-\log_{10}$(p-value). The integration scheme of multi-omics data is depicted in **Fig. S1**.

2.7. Statistics

Significance in the locomotor response test was analyzed using one-way analysis of variance with Dunnett's post-hoc test and was assessed with the criteria of a p-value < 0.05. Statistical analysis was performed using SigmaPlot v13 (Systat Software, San Jose, CA, USA). Significance in the omics analysis (p-value < 0.05) was evaluated with tools that were used for the analysis of each omics.

3. Results

3.1. Developmental, morphological, and behavioral impacts of PFOS

Developmental toxicity in zebrafish larvae was evaluated at 0.1–20 μM PFOS (**Fig. S2**). All concentrations showed no significance in mortality, whereas a significant malformation was observed at 20 μM but was only 17.2%. Malformed larvae exhibited pericardial and yolk sac edema, hematoma, and axis curvature.

In the locomotor response by light/dark transitions, the total distance was altered in proportion to the PFOS concentrations, which indicated hyperactivity and hypoactivity in light and dark conditions, respectively (Fig. 1**A**). The changes of total distance moved over time were described in Fig. S3. Exposure to 5 μM PFOS significantly decreased swimming movement during the first dark phase and significantly increased swimming movement during the second light phase. At 10 and 20 μM PFOS, the significant changes of the behavior activity were observed in all light conditions. Swimming behavior was examined regarding three types of speeds (Fig. 1**B**). During the light cycle, all types of movement, freezing, cruising, and bursting, were increased at the exposure concentrations of ≥ 5 μM; notably, the radar graph leaned toward the bursting movement. During the dark cycle, three kinds of movements significantly reduced at 10 and 20 μM PFOS (Fig. 1**C**). The behavior at bursting, cruising, and freezing speeds was altered in proportion to the increasing PFOS concentration. Excluding 20 μM concentration with high malformation, the omics analysis was carried out at ≤ 10 μM PFOS.

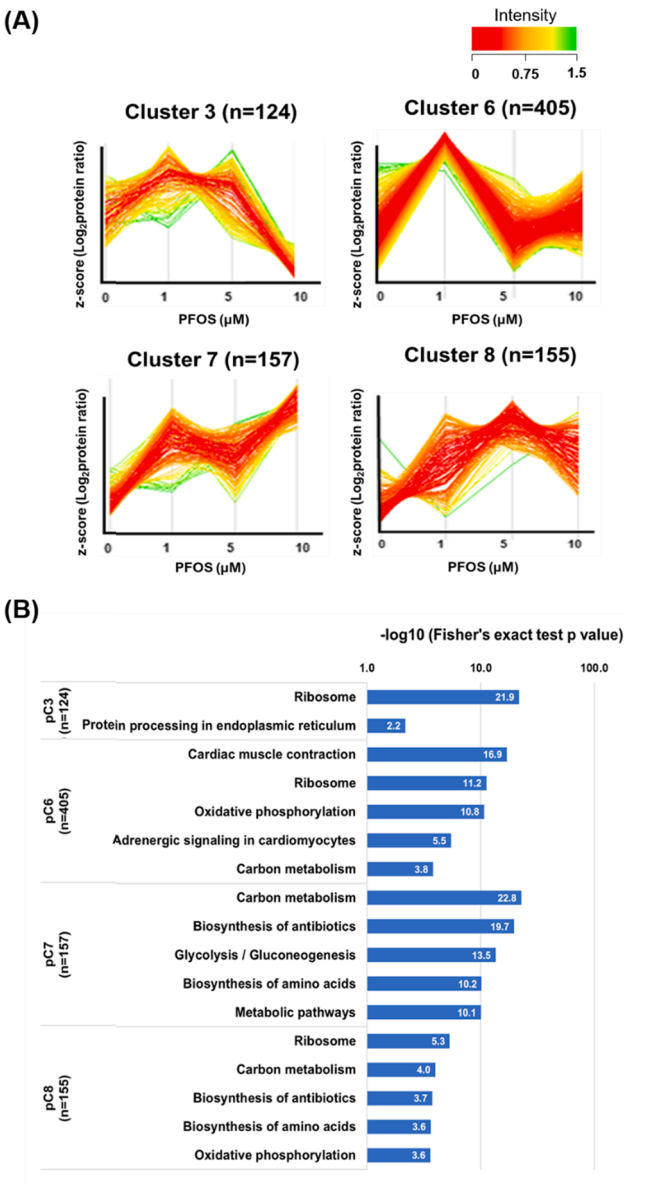

Fig. 3. Proteomic alteration. (A) Dynamic changes in proteomics and (B) significant pathways in proteomic clusters are exhibited. Among all clusters shown in **Fig. S6**, representative clusters that were obviously changed at PFOS 10 μM are shown.

3.2. Alterations in the transcriptomic profile

Of the 32,520 genes that were identified, 405 genes were significantly affected. At 1, 5, and 10 μM PFOS, the number of DEGs was identified to be 44, 37, and 359, respectively, of which up-regulated DEGs were 18, 14, and 247, and down-regulated DEGs were 26, 23, and 112 (Fig. 2**A and** Fig. S4**A**). The heatmap of the gene expression showed a rapid change at 10 μM PFOS (Fig. 2**B and** Fig. S4**B**). The Venn diagram revealed that > 30% of DEGs at 1 and 5 μM overlapped with DEGs at 10 μM. The detailed information on the common and specific DEGs at all PFOS concentrations was provided in the Supplementary File

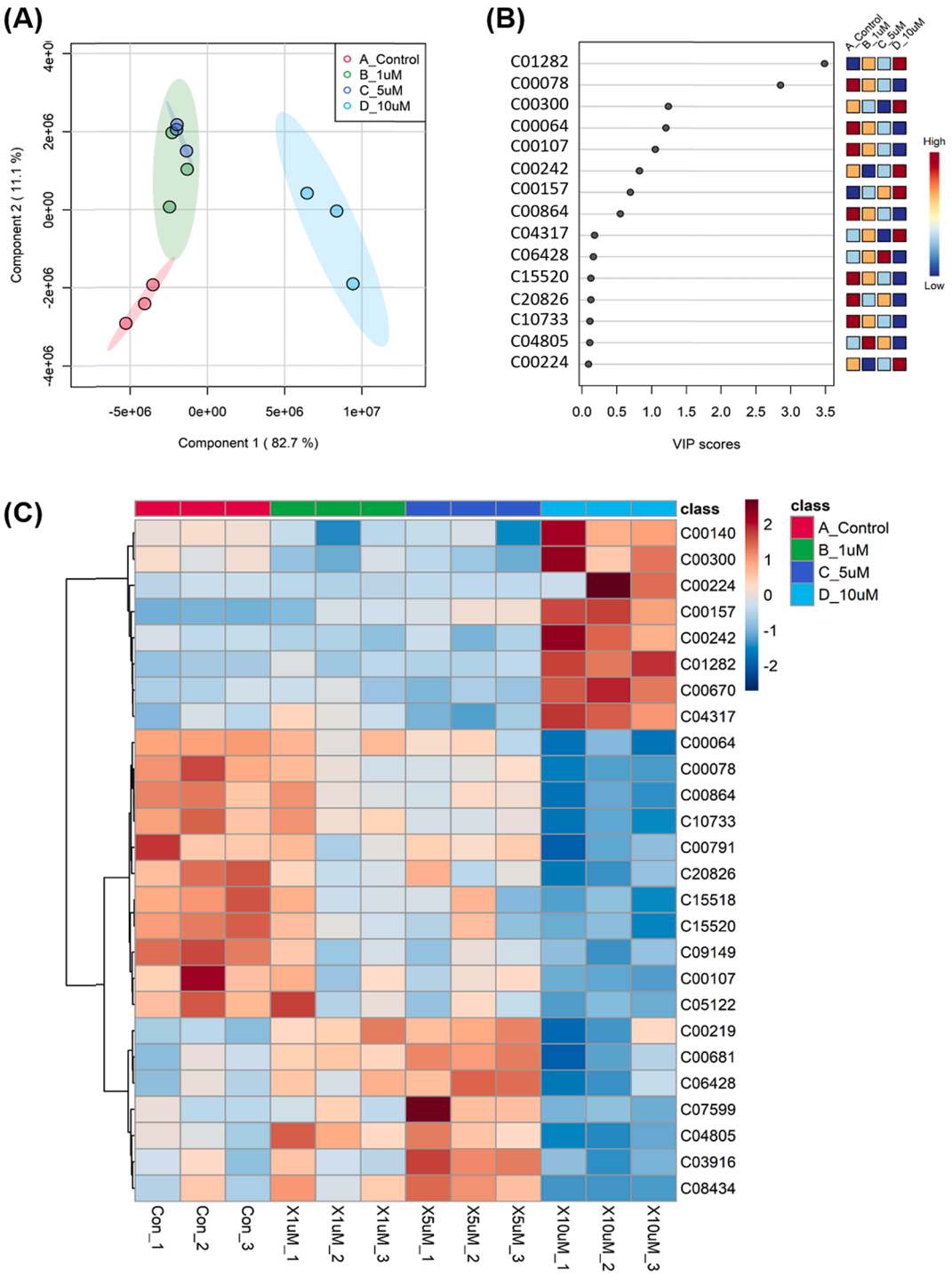

Fig. 4. Metabolomic alteration. (A) PLS-DA, (B) PLS-DA VIP score plots, and (C) heat map of differentially expressed metabolites (DEMs) of zebrafish larvae exposed to PFOS. Different concentrations in (A) and (C) are distinguished as the control (red), 1 μM (green), 5 μM (navy blue), and 10 μM (sky blue). Expression was represented with z-score (relatively up-regulated: *red* and down-regulated: *blue* among groups). The full name and KEGG ID of DEMs are indicated in **Table S3**. (For interpretation of the references to color in this figure legend, the reader is referred to the web version of this article.)

1. The expression patterns of DEGs were distinguished into three clusters (transcriptomic Clusters 1–3 [tCluster 1–3]) (Fig. 2**C**). First, tCluster 1 is a group of genes whose expression increased at 1 and 10 μM PFOS, as it was associated with chemokine activity. tCluster 2 is a group of genes whose expression was down-regulated obviously at 10 μM PFOS and is involved in vitamin transmembrane transporter activity, positive regulation of the nucleotide biosynthetic process, cortical granule, and heme binding. tCluster 3 is a group of genes whose expression was up-regulated rapidly at 10 μM PFOS and is involved in gamma-glutamylaminecyclotransferase activity, autophagosome membrane, ferrous iron binding, insulin-like growth factor 1 binding, sterol biosynthetic process, and peroxidase activity mechanisms. qRT-PCR was performed to verify the transcriptomic data, which were, consequently, compatible with RNA-seq (Fig. S5**A**).

3.3. Alterations in the proteomic profile

The numbers of identified proteins were approximately 1,200 in ≥

Table 1
Pathways related to differentially expressed metabolites.

Pathway	*p*-value
Glycerophospholipid metabolism	< 0.001 *
Alanine, aspartate, and glutamate metabolism	< 0.001 *
Purine metabolism	< 0.001 *
Tryptophan metabolism	< 0.001 *
Arachidonic acid metabolism	< 0.001 *
Primary bile acid biosynthesis	< 0.001 *
Sulfur metabolism	0.016
Ether lipid metabolism	0.018
Arginine and proline metabolism	0.029
Amino sugar and nucleotide sugar metabolism	0.037

Asterisk (*) denotes the statistical significance.

20 larvae, and the optimized number of larvae was determined to be 20 (**Table S2**). We confirmed that the technical correlations of the TMT quantitation were 0.661–0.786 (**Fig. S5B**). A total of 1,072 proteins was identified, and of these, 897 proteins (83.7%) could be quantified. Out of these proteins, the number of DEPs at 1, 5, and 10 μM was confirmed to be 32, 58, and 53, respectively. The quantified 897 proteins were analyzed through the volcano plot and their expression pattern was classified into eight proteomic Clusters (pClusters) (**Fig. S6**). Among all pClusters (Fig. 3), pCluster 3 showed the pattern of increasing at 1 and 5 μM and decreasing at 10 μM, which were attributed to the ribosome pathway. In pCluster 6, the protein expression levels increased clearly at 1 μM and were involved in cardiac muscle contraction, oxidative phosphorylation, and adrenergic signaling in cardiomyocytes. The proteins in pClusters 7 and 8 tended to increase at 1 to 10 μM and were involved in carbon metabolism, glycolysis/gluconeogenesis, and biosynthesis of amino acids.

3.4. Alterations in the metabolomic profile

Given the results shown for the similar number of identified metabolites at ≥ 50, the appropriate number of larvae was determined to be 50 (**Fig. S7**). A total of 169 metabolites was identified and quantified after merging the MS feature and metabolite identification. Finally, 26 metabolites were selected as DEMs based on statistical test (**Table S3**). In the PLS-DA score plot, the metabolite profile of the PFOS-treated group was clearly separated into the control and exposure groups. The metabolite profiles of 1 and 5 μM PFOS overlapped each other but they were remarkably differentiated from 10 μM PFOS (Fig. 4**A**). This result indicated a large fluctuation of the metabolite profile at 10 μM PFOS. In the PLS-DA VIP score plot, the metabolites of 1-acyl-2-oleoyl-*sn*-glycero-3-phosphocholine, L-tryptophan, creatine, L-glutamine, and dipeptide were distinctive (Fig. 4**B**). DEM-based hierarchical clustering analysis revealed three groups (Fig. 4**C**). In proportion with the increasing PFOS concentration, the expression level of the metabolites of metabolomic Cluster 1 (mCluster 1) increased, whereas that of mCluster 2 decreased. mCluster 3 included metabolites that were up-regulated at 5 μM and down-regulated at 10 μM. mCluster 1 was mainly composed of lipids such as glycerophosphocholine and phosphatidylcholine. mCluster 2 is composed of metabolites associated with amino acids metabolism or bile acid metabolism. mCluster 3 also contained lipid-related metabolites and molecules such as oxypurinol and N_6-methyladenine. The pathways that were analyzed by all DEMs were associated with amino acid and lipid metabolisms, as well as purine, sulfur, amino-, and nucleotide-sugar metabolisms (Table 1).

3.5. Multi-layered molecular alterations by PFOS exposure

The transcriptome, proteome, and metabolome data acquired from zebrafish larvae were integrated to unravel the underlying molecular mechanisms of PFOS-induced neurotoxicity. The topological network between biomolecules was described (Fig. 5**A**) and classified into eight integrated clusters (iClusters 1–8). The top six pathways in each iCluster were described in Fig. 5**B**. iCluster 1 (consisting of one gene and one protein) was not examined due to insufficient biomolecules for pathway analysis. iCluster 2 (consisting of 27 genes and 28 proteins) included Ca^{2+} binding-related pathways. iCluster 3 (consisting of 75 genes, nine proteins, and four metabolites) included pathways related to producing the resource substances of neurotransmission. iCluster4 (consisting of 16 genes and 32 proteins) was associated with Ca^{2+}-regulated muscle contraction. iCluster 5 (consisting of 35 genes, eight proteins, and three metabolites) included pathways of proteasome-linked actin-binding protein and amino acid metabolisms. iCluster 6 (consisting of 123 genes, five proteins, and seven metabolites) was associated with lipid metabolism and cell proliferation and apoptosis. iCluster 7 (consisting of 12 genes, one protein, and six metabolites) contained phospholipid-translocating ATPase activity mechanisms. iCluster 8 (consisting of 103 genes, 20 proteins, and six metabolites) was associated with lipid and immunological metabolisms. The total pathways obtained from integrated omics are provided in **Table S4**.

4. Discussion

Behavior assessment revealed that PFOS exposure induced neurobehavioral changes in response to light stimulation in zebrafish. Although both hyperactivity (Gaballah et al., 2020) and hypoactivity (Ulhaq et al., 2013) were reported at exposure concentrations of 0.2–20 μM, our observation agrees with other studies reporting that the locomotor behavior is affected by PFOS (Kim et al., 2020; Ulhaq et al., 2013). The type of behavioral alteration was primarily bursting movement, which is a high-speed swimming movement, in proportion to PFOS concentrations. On the basis of the behavioral results, the developmental neurotoxicity of PFOS was confirmed.

On a string of molecular levels, transcriptomics revealed that the DEGs are associated with the pathways of neurological function, which were remarkably significant at 10 μM PFOS. In tCluster 1, chemokine ligand 8 (CXCL8), which is also known as interleukin 8, is released by astrocytes and activated to protect the brain at the initiation of neuronal damage (Azizi et al., 2015). CXCL8 elevation was reported in patients with brain injury, BBB dysfunction, or dysregulation of neurotransmitter release (Semple et al., 2010). In the vitamin transmembrane transporter activity of tCluster 2, solute carrier family 52, member 3 (SLC52A3), an orthologous gene of zebrafish *si:ch73-196 l6.5*, is involved in transferring riboflavin, namely, vitamin B2. Deficiency or mutations of SLC52A3, which is a brain-specific transporter, are linked to motor neuron disease (Canchi et al., 2019). In the heme-binding pathway, CYP27B1 contributes toward the vitamin D metabolism, which is important for neural differentiation and maturation and the synthesis of neurotransmitters such as acetylcholine and gamma aminobutyric acid (GABA). Therefore, vitamin D deficiency can cause neurological disease (Moretti et al., 2018). Further, PFOS exposure down-regulated the nitric oxide (NO) synthase 2 gene, which participates in NO production in the cytosol of glial cells. NO functions as a signaling molecule in the brain, and dysregulation of NO signaling leads to neurodevelopmental and neurobehavioral impairment (Tripathi et al., 2020). In the tCluster 3, the ferrous ion-binding pathway was confirmed and contained DEG-encoding ferritin, which is an iron storage protein. Along with ferritin, prostaglandin-endoperoxide synthase 2, which belongs to the peroxidase pathway, is involved in ferroptosis. Ferroptosis contributes to neuronal death and is linked to various brain diseases (Yao et al., 2021). Other DEGs are associated with various pathways of liver development, peroxidation, oxidative stress, and cellular signaling. Importantly, PFOS affected genes that are engaged in neurological damage-linked pathways. Although DEGs mostly enriched at 10 μM were first discussed, DEGs that are associated with central nervous system disease (Dalakas et al., 2020) and neuropeptide production (Podvin et al., 2018) were also observed at 5 μM, such as complement component 7b and si:dkey-26 g8.5, an orthologous zebrafish gene of cathepsin V and L, attributable

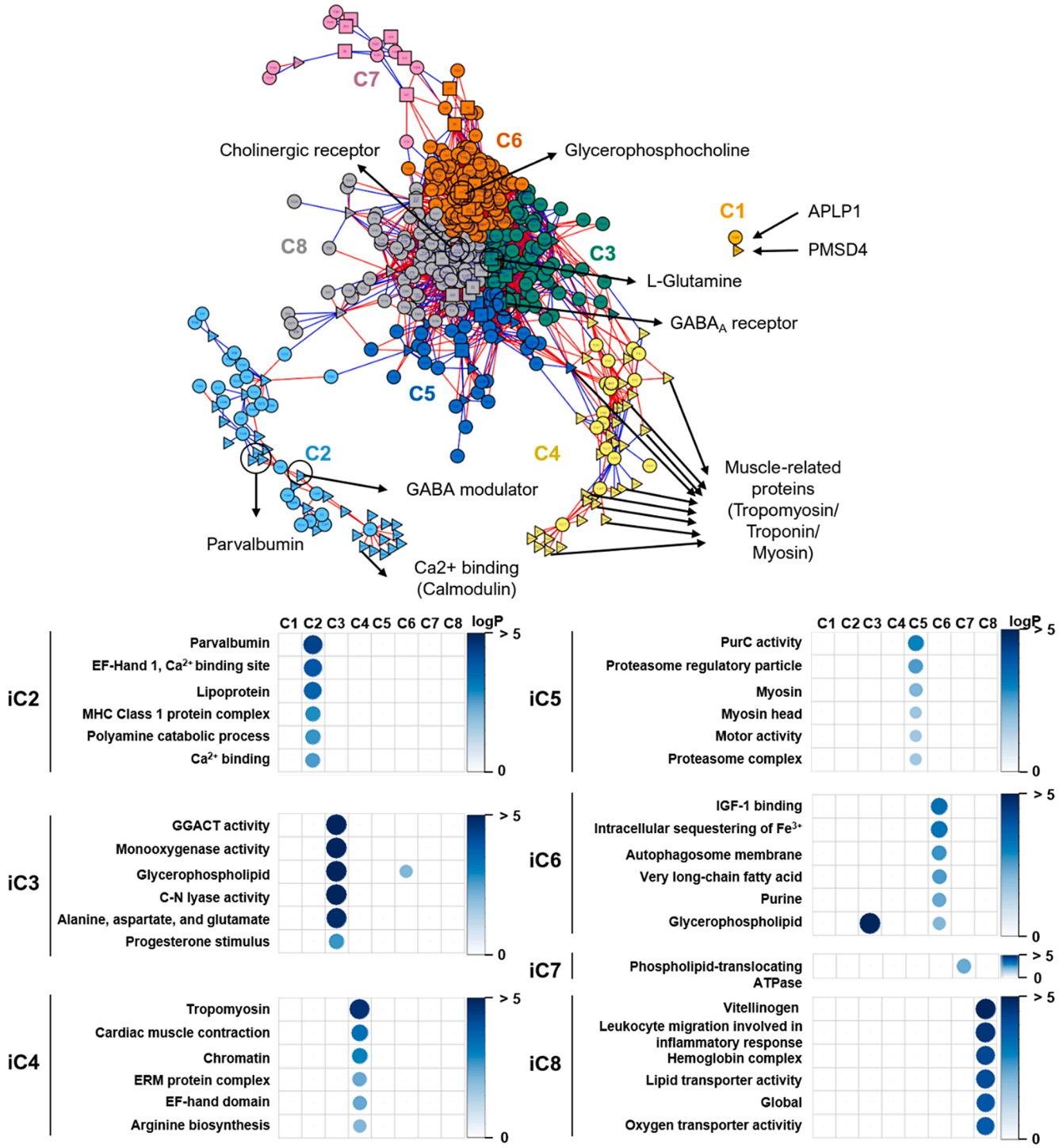

Fig. 5. Data-driven integration of multi-omics. (A) Integrative networks of biomolecules are analyzed using metabolomics (*square*), proteomics (*triangle*), and transcriptomics (*circle*). The clusters consist of highly correlated biomolecules and are distinguished by colors. (B) Top six pathways in integrated Clusters 2–8 are described by both circle size and color saturation which indicate − log (*p*-value (P)). All pathways of each cluster are described in **Table S4**.

to the neurobehavioral alteration at 5 μM.

In proteomics, as for protein factors related to neurotoxicity following PFOS exposure, parvalbumin (PV) in pCluster 6 significantly increased at 1 μM PFOS. PV, which is a Ca^{2+} binding protein with low-molecular-weight, is found in γ-GABA-type interneurons in the nervous system (Ferguson and Gao, 2018) and plays a role as a regulator of neuronal Ca^{2+} signals (Lauber et al. 2018). Increased PV expression stimulates GABAnergic neurotransmission and alleviates neurological impairment, which suggests that 1 μM PFOS activates a defensive reaction to neurological adverse effects. DEPs related to neurological effects were also found in the pClusters 3, 7 and 8, showing the obvious perturbation by 10 μM PFOS. These DEPs were associated with the ryanodine receptor, skeletal muscle components, and Rab proteins. The ryanodine receptor, a class of Ca^{2+} channel, regulates Ca^{2+} concentrations in the neuromuscular junction and contributes toward the signaling of muscles and neurons. The dysregulation of ryanodine receptors develops neurodegenerative disease (Kushnir et al., 2018). The DEPs associated with ryanodine receptor and muscle components were

also found at 5 μM where zebrafish behavior was significantly affected. In addition, Rab proteins play a role in regulating the signaling of neurotrophin receptors that are responsible for neuronal development (Bucci et al., 2014). Proteomic alterations therefore showed that PFOS exposure causes abnormal neurological regulation in developing zebrafish embryos.

Metabolomics revealed multi-functional metabolic pathways, such as energy metabolism, cellular signaling, and neurological regulation. Arachidonic acid, which is a significant DEM, is an important precursor to inflammation mediators, including prostaglandin and leukotriene (Granström et al., 1984). Disturbance of arachidonic acid metabolism is associated with neuroinflammation. Further, PFOS exposure decreased tryptophan, which is a substrate produced during the synthesis of the neurotransmitter serotonin, which plays an integrative role in behavioral response. Dysregulation of tryptophan metabolism was associated with central nervous system disease (Lovelace et al., 2017). We therefore speculate that the significant behavior alterations were attributed to reduction of L-tryptophan. Exposure to PFOS significantly affected glycerophospholipid metabolism, which contains a biosynthesis of choline. Glycerophosphocholine and phosphatidylcholine are endogenous precursors of choline that is required for the production of acetylcholine neurotransmitter. These metabolites were significantly increased at 10 μM PFOS. The elevation of glycerophosphocholine was found in patients with neurological disorders, e.g., Alzheimer's disease (Walter et al., 2004). As a metabolite of alanine, aspartate, and glutamate metabolisms, L-glutamine was significantly reduced at 5 and 10 μM PFOS. L-glutamine is essential for mediating glutamatergic and GABAergic transmissions as a precursor of glutamate and GABA neurotransmitters. Inhibition of glutamine synthesis can lead to neuronal dysfunction (Albrecht et al., 2010). In fact, L-glutamine is essential for metabolic pathways, such as glycolysis. As a primary bile acid, taurocholic acid was significantly reduced at 10 μM PFOS. Overall, metabolomic profiles revealed that PFOS widely disrupted the basal energy metabolisms and nervous system.

Integrated omics analysis was performed to merge the outcomes of individual omics and to identify molecular perturbations that are common among the three omics, which is efficient for interpreting the molecular mechanisms of PFOS neurotoxicity. The unique pathways of integrated omics were discovered through comparison with individual omics. In iCluster 2, dysregulation of the polyamine catabolic process was identified. Polyamine is abundant in the brain and participates in the maturation and plasticity of neurons via polyamination of tubulin. Polyaminated tubulins stabilize the axonal microtubule; therefore, they are critical for maintaining the neuronal function and structure. Abnormal polyamine catabolism was reported to increase cerebellar dysfunction and neuroinflammation (Zahedi et al., 2020). Therefore, PFOS exposure might disturb the formation and development of neurons. iClusters 4 and 5 included the pathways that are involved in Ca^{2+}-linked neuromuscular pathways, such as cardiac muscle contraction, tropomyosin, and myosin. The muscle-related biomolecules in iCluster 4 engage in both skeletal and cardiac muscle contraction. Muscle contraction occurs with a stimulated efflux of Ca^{2+}, binding of Ca^{2+} with troponin, and attachment of the myosin head to actin (Kuo and Ehrlich 2015). These procedures were identified by integrated omics, suggesting that PFOS influences the regulation of muscle nerves that are responsible for motor behavior (Dubińska-Magiera et al., 2016). In addition, the endoplasmic reticulum membrane protein, which participates in a Ca^{2+} signaling, was disturbed. Ca^{2+}-dependent pathways such as the Ca^{2+} binding site and the MHC Class I protein complex were also identified. Ca^{2+} plays a crucial role as a regulator of nerve stimulation and transmission (Zündorf and Reiser, 2011). Our findings thus suggested that PFOS can impede overall Ca^{2+} signal-linked pathways and lead to the impaired nervous system. In iCluster 7, phospholipid-translocating ATPase was influenced by PFOS. ATP8A1 belonging to this pathway was involved in synaptic strength and social behavior in mice (Kerr et al., 2016). Leukocyte migration involved in the inflammatory response pathway was also found in iCluster 8. Leukocyte migration into the central nervous system across the BBB is associated with neuroinflammation. PFOS was previously reported to pass through BBB into the brain (Andersen et al., 2006) and to activate the proinflammatory markers in rat brain (Zeng et al., 2011). Therefore, leukocyte migration was expected to be overexpressed due to neuroinflammation induced by PFOS.

Integrated omics provided multifaceted mechanisms by which PFOS exerted negative effects on the formation and structure of neurons, neuroinflammation, and regulation of Ca^{2+} signaling-linked pathways, which explains the observed behavioral alteration and neurotoxicity. It is notable that the neuronal formation-associated pathway was identified only by integrated omics, and Ca^{2+} signaling-linked pathways were identified more from integrated omics than individual omics. Integrated omics analysis is more effective for exploring the decisive pathways associated with developmental neurotoxicity. The molecular pathways found by integrated omics were comparable with the mechanisms of PFOS-induced neurotoxicity such as oxidative stress, neuroinflammation, abnormalities of synaptic formation and plasticity, dysregulation of Ca^{2+} homeostasis, and alteration of neurotransmitter levels as proposed by literature review (Zeng et al. 2019). Therefore, our study provides insights into researches using integrated omics analysis for identifying significant toxicity mechanisms of PFOS, which can be applied to compare relative toxicity potencies of emerging PFAS or PFOS alternatives.

CRediT authorship contribution statement

Hyojin Lee: Investigation, Visualization, Formal analysis, Writing - original draft, Writing - review & editing. **Eun Ji Sung:** Investigation, Visualization, Writing - original draft. **Seungwoo Seo:** Investigation, Visualization, Writing - original draft. **Eun Ki Min:** Investigation, Visualization. **Ji-Young Lee:** Conceptualization, Supervision. **Ilseob Shim:** Conceptualization, Supervision. **Pilje Kim:** Conceptualization, Supervision. **Tae-Young Kim:** Conceptualization, Supervision, Writing - review & editing. **Sangkyu Lee:** Conceptualization, Supervision, Writing - review & editing. **Ki-Tae Kim:** Conceptualization, Supervision, Writing - review & editing.

Declaration of Competing Interest

The authors declare that they have no known competing financial interests or personal relationships that could have appeared to influence the work reported in this paper.

Acknowledgments

This study was supported by a grant from the National Institute of Environmental Research (NIER), the Republic of Korea (NIER-SP2020-257). This research was supported by Basic Science Research Capacity Enhancement Project through Korea Basic Science Institute (National research Facilities and Equipment Center) grant funded by the Ministry of Education (grant No.2019R1A6C1010001).

Appendix A. Supplementary material

Supplementary data to this article can be found online at https://doi.org/10.1016/j.envint.2021.106802.

References

Albrecht, J., Sidoryk-Węgrzynowicz, M., Zielińska, M., Aschner, M., 2010. Roles of glutamine in neurotransmission. Neuron Glia Biol. 6 (4), 263–276.

Andersen, M.E., Clewell 3rd., H.J., Tan, Y.M., Butenhoff, J.L., Olsen, G.W., Andersen, M. E., 2006. Pharmacokinetic modeling of saturable, renal resorption of perfluoroalkylacids in monkeys–probing the determinants of long plasma half-lives. Toxicology 227, 156–164.

Azizi, G., Navabi, S.S., Al-Shukaili, A., Seyedzadeh, M.H., Yazdani, R., Mirshafiey, A., 2015. The role of inflammatory mediators in the pathogenesis of Alzheimer's disease. Sultan Qaboos Univ. Med. J. 15 (3), e305–e316.

Bucci, C., Alifano, P., Cogli, L., 2014. The role of rab proteins in neuronal cells and in the trafficking of neurotrophin receptors. Membranes (Basel) 4 (4), 642–677.

Buesen, R., Chorley, B.N., da Silva Lima, B., Daston, G., Deferme, L., Ebbels, T., Gant, T. W., Goetz, A., Greally, J., Gribaldo, L., Hackermüller, J., Hubesch, B., Jennen, D., Johnson, K., Kanno, J., Kauffmann, H.M., Laffont, M., McMullen, P., Meehan, R., Pemberton, M., Perdichizzi, S., Piersma, A.H., Sauer, U.G., Schmidt, K., Seitz, H., Sumida, K., Tollefsen, K.E., Tong, W., Tralau, T., van Ravenzwaay, B., Weber, R.J.M., Worth, A., Yauk, C., Poole, A., 2017. Applying 'omics technologies in chemicals risk assessment: Report of an ECETOC workshop. Regul. Toxicol. Pharmacol. 91 (Suppl 1), S3–S13.

Canchi, S., Raao, B., Masliah, D., Rosenthal, S.B., Sasik, R., Fisch, K.M., De Jager, P.L., Bennett, D.A., Rissman, R.A., 2019. Integrating gene and protein expression reveals perturbed functional networks in Alzheimer's disease. Cell. Rep. 28 (4), 1103–1116.e4.

Canzler, S., Schor, J., Busch, W., Schubert, K., Rolle-Kampczyk, U.E., Seitz, H., Kamp, H., von Bergen, M., Buesen, R., Hackermüller, J., 2020. Prospects and challenges of multi-omics data integration in toxicology. Arch. Toxicol. 94 (2), 371–388.

Chen, N., Li, J., Li, D., Yang, Y., He, D., 2014. Chronic exposure to perfluorooctane sulfonate induces behavior defects and neurotoxicity through oxidative damages, in vivo and in vitro. PLoS One 9 (11), e113453.

Cui, L., Zhou, Q.-F., Liao, C.-Y., Fu, J.-J., Jiang, G.-B., 2009. Studies on the toxicological effects of PFOA and PFOS on rats using histological observation and chemical analysis. Arch. Environ. Contam. Toxicol. 56 (2), 338–349.

d'Amora, M., Giordani, S., 2018. The utility of zebrafish as a model for screening developmental neurotoxicity. Front. Neurosci. 12, 976.

Dalakas, M.C., Alexopoulos, H., Spaeth, P.J., 2020. Complement in neurological disorders and emerging complement-targeted therapeutics. Nat. Rev. Neurol. 16 (11), 601–617.

Dubińska-Magiera, M., Daczewska, M., Lewicka, A., Migocka-Patrzałek, M., Niedbalska-Tarnowska, J., Jagla, K., 2016. Zebrafish: A model for the study of toxicants affecting muscle development and function. Int. J. Mol. Sci. 17 (11), 1941. https://doi.org/10.3390/ijms17111941.

Ferguson, B.R. and W.J. Gao, P.V., 2018. Interneurons: Critical regulators of E/I balance for prefrontal cortex-dependent behavior and psychiatric disorders. Front. Neural. Circuits 12, 37.

Gaballah, S., Swank, A., Sobus, J.R., Howey, X.M., Schmid, J., Catron, T., McCord, J., Hines, E., Strynar, M., Tal, T., 2020. Evaluation of developmental toxicity, developmental neurotoxicity, and tissue dose in zebrafish exposed to GenX and other PFAS. Environ. Health Perspect. 128 (4), 047005. https://doi.org/10.1289/EHP5843.

Gowda, H., Ivanisevic, J., Johnson, C.H., Kurczy, M.E., Benton, H.P., Rinehart, D., Nguyen, T., Ray, J., Kuehl, J., Arevalo, B., Westenskow, P.D., Wang, J., Arkin, A.P., Deutschbauer, A.M., Patti, G.J., Siuzdak, G., 2014. Interactive XCMS online: simplifying advanced metabolomic data processing and subsequent statistical analyses. Anal. Chem. 86 (14), 6931–6939.

Granström, E., 1984. The arachidonic acid cascade. The prostaglandins, thromboxanes and leukotrienes. Inflammation. 8 (S1), S15–S25.

Jin, M., Li, N., Sheng, W., Ji, X., Liang, X., Kong, B., Yin, P., Li, Y., Zhang, X., Liu, K. Toxicity of different zinc oxide nanomaterials and dose-dependent onset and development of Parkinson's disease-like symptoms induced by zinc oxide nanorods. Environ. Int. 146, 106179.

Johansson, N., Fredriksson, A., Eriksson, P., 2008a. Neonatal exposure to perfluorooctane sulfonate (PFOS) and perfluorooctanoic acid (PFOA) causes neurobehavioural defects in adult mice. Neurotoxicology 29 (1), 160–169.

Johansson, N., Viberg, H., Fredriksson, A., Eriksson, P., 2008b. Neonatal exposure to deca-brominated diphenyl ether (PBDE 209) causes dose-response changes in spontaneous behaviour and cholinergic susceptibility in adult mice. Neurotoxicology 29 (6), 911–919.

Kerr, D.J., Marsillo, A., Guariglia, S.R., Budylin, T., Sadek, R., Menkes, S., Chauhan, A., Wen, G.Y., McCloskey, D.P., Wieraszko, A., Banerjee, P., 2016. Aberrant hippocampal Atp8a1 levels are associated with altered synaptic strength, electrical activity, and autistic-like behavior. Biochim. Biophys. Acta. 1862 (9), 1755–1765.

Kim, S., Stroski, K.M., Killeen, G., Smitherman, C., Simcik, M.F., Brooks, B.W., 2020. 8:8 Perfluoroalkyl phosphinic acid affects neurobehavioral development, thyroid disruption, and DNA methylation in developing zebrafish. Sci. Total Environ. 736, 139600. https://doi.org/10.1016/j.scitotenv.2020.139600.

Kimmel, C.B., Ballard, W.W., Kimmel, S.R., Ullmann, B., Schilling, T.F., 1995. Stages of embryonic development of the zebrafish. Dev. Dyn. 203 (3), 253–310.

Kuo, I.Y., Ehrlich, B.E., 2015. Signaling in muscle contraction. Cold Spring Harb. Perspect. Biol. 7 (2), a006023.

Kushnir, A., Wajsberg, B., Marks, A.R., 2018. Ryanodine receptor dysfunction in human disorders. Biochim. Biophys. Acta. Mol. Cell Res. 1865 (11), 1687–1697.

Kwon, B.G., Lim, H.J., Na, S.H., Choi, B.I., Shin, D.S., Chung, S.Y., 2014. Biodegradation of perfluorooctanesulfonate (PFOS) as an emerging contaminant. Chemosphere 109, 221–225.

Lauber, E., Filice, F., Schwaller, B., 2018. Dysregulation of parvalbumin expression in the cntnap2-/- mouse model of autism spectrum disorder. Front. Mol. Neurosci. 11, 262.

Lee, H., Gao, Y., Ko, E., Lee, J., Lee, H.K., Lee, S., Choi, M., Shin, S., Park, Y.H., Moon, H. B., Uppal, K., Kim, K.T., 2021. Nonmonotonic response of type 2 diabetes by low concentration organochlorine pesticide mixture: Findings from multi-omics in zebrafish. J. Hazard. Mater. 416, 125956. https://doi.org/10.1016/j.jhazmat.2021.125956.

Lee, H., Lee, J., Choi, K., Kim, K.T., 2019. Comparative analysis of endocrine disrupting effects of major phthalates in employed two cell lines (MVLN and H295R) and embryonic zebrafish assay. Environ. Res. 172, 319–325.

Lee, Y.M., Lee, J.Y., Kim, M.K., Yang, H., Lee, J.E., Son, Y., Kho, Y., Choi, K., Zoh, K.D., 2020. Concentration and distribution of per- and polyfluoroalkyl substances (PFAS) in the Asan Lake area of South Korea. J. Hazard. Mater. 381, 120909.

Lin, Y., Ruan, T., Liu, A., Jiang, G., 2017. Identification of novel hydrogen-substituted polyfluoroalkyl ether sulfonates in environmental matrices near metal-plating facilities. Environ. Sci. Technol. 51 (20), 11588–11596.

Lovelace, M.D., Varney, B., Sundaram, G., Lennon, M.J., Lim, C.K., Jacobs, K., Guillemin, G.J., Brew, B.J., 2017. Recent evidence for an expanded role of the kynurenine pathway of tryptophan metabolism in neurological diseases. Neuropharmacology. 112, 373–388.

Martínez, Rubén, Navarro-Martín, Laia, Luccarelli, Chiara, Codina, Anna E., Raldúa, Demetrio, Barata, Carlos, Tauler, Romà, Piña, Benjamin, 2019. Unravelling the mechanisms of PFOS toxicity by combining morphological and transcriptomic analyses in zebrafish embryos. Sci. Total Environ. 674, 462–471.

Menger, F., Pohl, J., Ahrens, L., Carlsson, G., Örn, S., 2020. Behavioural effects and bioconcentration of per- and polyfluoroalkyl substances (PFASs) in zebrafish (Danio rerio) embryos. Chemosphere 245, 125573.

Moody, C.A., Martin, J.W., Kwan, W.C., Muir, D.C., Mabury, S., 2002. Monitoring perfluorinated surfactants in biota and surface water samples following an accidental release of fire-fighting foam into Etobicoke Creek. Environ. Sci. Technol. 36, 545–551.

Moretti, R., Morelli, M.E., Caruso, P., 2018. Vitamin D in neurological diseases: a rationale for a pathogenic impact. Int. J. Mol. Sci. 19 (8), 2245. https://doi.org/10.3390/ijms19082245.

Olsen, G.W., Mair, D.C., Lange, C.C., Harrington, L.M., Church, T.R., Goldberg, C.L., Herron, R.M., Hanna, H., Nobiletti, J.B., Rios, J.A., Reagen, W.K., Ley, C.A., 2017. Per- and polyfluoroalkyl substances (PFAS) in american red cross adult blood donors, 2000–2015. Environ. Res. 157, 87–95.

Ortiz-Villanueva, E., Jaumot, J., Martínez, R., Navarro-Martín, L., Piña, B., Tauler, R., 2018. Assessment of endocrine disruptors effects on zebrafish (Danio rerio) embryos by untargeted LC-HRMS metabolomic analysis. Sci. Total Environ. 635, 156–166.

Perez-Riverol, Y., Csordas, A., Bai, J., Bernal-Llinares, M., Hewapathirana, S., Kundu, D. J., Inuganti, A., Griss, J., Mayer, G., Eisenacher, M., Pérez, E., Uszkoreit, J., Pfeuffer, J., Sachsenberg, T., Yilmaz, S., Tiwary, S., Cox, J., Audain, E., Walzer, M., Jarnuczak, A.F., Ternent, T., Brazma, A., Vizcaíno, J.A., 2019. The PRIDE database and related tools and resources in 2019: improving support for quantification data. Nucleic Acids Res. 47 (D1), D442–D450.

Podvin, S., Wojnicz, A., Hook, V., 2018. Human brain gene expression profiles of the cathepsin V and cathepsin L cysteine proteases, with the PC1/3 and PC2 serine proteases, involved in neuropeptide production. 4, e00673.

Semple, B.D., Kossmann, T., Morganti-Kossmann, M.C., 2010. Role of chemokines in CNS health and pathology: a focus on the CCL2/CCR2 and CXCL8/CXCR2 networks. 30, 459-473.

Tran, C.M., Do, T.N., Kim, K.T., 2021. Comparative analysis of neurotoxicity of six phthalates in zebrafish embryos. Toxics 9, 5.

Tripathi, M.K., Kartawy, M., Amal, H., 2020. The role of nitric oxide in brain disorders: Autism spectrum disorder and other psychiatric, neurological, and neurodegenerative disorders. Redox Biol. 34, 101567.

Tsuda, S., 2016. Differential toxicity between perfluorooctane sulfonate (PFOS) and perfluorooctanoic acid (PFOA). J. Toxicol. Sci. 41, SP27-SP36.

Ulhaq, M., Orn, S., Carlsson, G., Morrison, D.A., Norrgren, L., 2013. Locomotor behavior in zebrafish (Danio rerio) larvae exposed to perfluoroalkyl acids. Aquat. Toxicol. 144–145, 332–340.

Uppal, K., Ma, C., Go, Y.M., Jones, D.P., Wren, J., 2018. xMWAS: a data-driven integration and differential network analysis tool. Bioinformatics 34, 701–702.

Valsecchi, S., Babut, M., Mazzoni, M., Pascariello, S., Ferrario, C., Felice, B., Bettinetti, R., Veyrand, B., Marchand, P., Polesello, S., 2021. Perfluoroalkyl substances (PFAS) in fish from European lakes: current contamination status, sources, and perspectives for monitoring. Environ Toxicol Chem. 40 (3), 656–676.

Walter, A., Korth, U., Hilgert, M., Hartmann, J., Weichel, O., Hilgert, M., Fassbender, K., Schmitt, A., Klein, J., 2004. Glycerophosphocholine is elevated in cerebrospinal fluid of Alzheimer patients. Neurobiol. Aging 25, 1299–1303.

Wu, Y., Zeng, J., Zhang, F., Zhu, Z., Qi, T., Zheng, Z., Lloyd-Jones, L.R., Marioni, R.E., Martin, N.G., Montgomery, G.W., Deary, I.J., Wray, N.R., Visscher, P.M., McRae, A. F., Yang, J., 2018. Integrative analysis of omics summary data reveals putative mechanisms underlying complex traits. Nat. Commun. 9, 918.

Yao, M.Y., Liu, T., Zhang, L., Wang, M.J., Yang, Y., Gao, J., 2021. Role of ferroptosis in neurological diseases. Neurosci. Lett. 747, 135614.

Yuan, Z., Shao, X., Miao, Z., Zhao, B., Zheng, Z., Zhang, J., 2018. Perfluorooctane sulfonate induced neurotoxicity responses associated with neural genes expression, neurotransmitter levels and acetylcholinesterase activity in planarians Dugesia japonica. Chemosphere 206, 150–156.

Zahedi, K., Brooks, M., Barone, S., Rahmati, N., Murray, S.T., Dunworth, M., Destefano-Shields, C., Dasgupta, N., Davidson, S., Lindquist, D.M., Fuller, C.E., Smith, R.D., Cleveland, J.L., Casero Jr., R.A., Soleimani, M., 2020. Ablation of polyamine catabolic enzymes provokes Purkinje cell damage, neuroinflammation, and severe ataxia. J. Neuroinflammation 17, 301.

Zeng, H.C., Zhang, L., Li, Y.Y., Wang, Y.J., Xia, W., Lin, Y., Wei, J., Xu, S.Q., 2011. Inflammation-like glial response in rat brain induced by prenatal PFOS exposure. Neurotoxicology 32, 130–139.

Zeng, Z., Song, B., Xiao, R., Zeng, G., Gong, J., Chen, M., Xu, P., Zhang, P., Shen, M., Yi, H., 2019. Assessing the human health risks of perfluorooctane sulfonate by in vivo and in vitro studies. Environ. Int. 126, 598–610.

Zhang, K., Liang, J., Brun, N.R., Zhao, Y., Werdich, A.A., 2021. Rapid zebrafish behavioral profiling assay accelerates the identification of environmental neurodevelopmental toxicants. Environ. Sci. Technol. 55, 1919–1929.

Zündorf, G., Reiser, G., 2011. Calcium dysregulation and homeostasis of neural calcium in the molecular mechanisms of neurodegenerative diseases provide multiple targets for neuroprotection. Antioxid. Redox Signal. 14, 1275–1288.